J. Opt. B: Quantum Semiclass. Opt. **2** (2000) 672–685. Printed in the UK PII: S1464-4266(00)12284-0

Observation of coherent backscattering of light by cold atoms

G Labeyrie†, C A Müller†, D S Wiersma†‡, Ch Miniatura† and R Kaiser†

† INLN UMR 6618 CNRS-UNSA, 1361 route des Lucioles, F-06560 Valbonne, France
‡ European laboratory for non-linear spectroscopy, and Instituto nazionale per la fisica della materia, Florence, Italy

Received 3 March 2000, in final form 12 July 2000

Abstract. Coherent backscattering (CBS) of light waves by a random medium is a signature of interference effects in multiple scattering. This effect has been studied in many systems ranging from white paint to biological tissues. Recently, we have observed CBS from a sample of laser-cooled atoms, a scattering medium with interesting new properties. In this paper we discuss various effects which have to be taken into account for a quantitative study of coherent backscattering of light by cold atoms.

Keywords: Coherent backscattering of light, cold atoms, magneto-optical trap

1. Introduction

A wave propagating in a strongly scattering random medium undergoes many scattering events and the memory of its initial direction is rapidly lost. This simple observation applies to many everyday life situations, like driving a car in thick fog. Understanding the rules of wave propagation in such media may have some interesting applications, e.g. in medical imaging or in mesoscopic physics.

Since the wave propagation can be seen as a random walk inside the medium, a diffusion picture seems appropriate. Neglecting all interference phenomena, one predicts a total transmission of the medium inversely proportional to the sample thickness (Ohm's law). However, interferences may have dramatic consequences, such as a vanishing diffusion constant: in this situation, the medium behaves like an insulator (strong or Anderson localization) [1] and its total transmission decreases exponentially with the sample's thickness. This prediction has triggered a renewal of interest in the study of multiple scattering, leading to experiments on strong localization of microwaves [2] and light [3]. A more accessible experimental situation is the so-called weak localization regime, where interferences already hamper the diffusion process. Coherent backscattering (CBS) is a spectacular manifestation of interference effects in this multiple-scattering regime, yielding an enhanced scattered intensity around the direction of backscattering. This phenomenon has been observed in a variety of systems [4].

Recently, we observed CBS of light from a sample of laser-cooled atoms [5]. Indeed, multiple scattering of light is known to exist in such samples since it eventually limits the atomic density achievable in magneto-optical traps (MOTs) [6]. Direct manifestations of multiple scattering of light in cold atoms such as 'radiation trapping' had already been observed [7], but our experiment now allows one to probe the interference effects in this situation. In this respect, CBS is a powerful tool for studying the properties of light scattered by cold atoms. Indeed, we observed some striking differences with what is reported in the literature for classical samples. In order to understand more precisely the physics underlying these differences, we have to analyse various effects, such as geometrical or polarization effects, which could modify the CBS signal even for classical samples such as a suspension of TiO_2 beads. The goal of this paper is to study such effects in order to point out behaviours connected to the internal structure of the atoms.

In section 2, we first recall the basic physics of CBS, with special attention being given to the parameters that determine the CBS cone shape. Section 3 is devoted to experiments with classical samples. After describing the detection setup, we discuss several effects that can affect the signal. We put an emphasis on the rather non-trivial problem of determining a precise value of the enhancement factor. Section 4 is dedicated to the experiment with cold atoms, including a description of the procedure to prepare the sample.

2. CBS

2.1. Principle of CBS

To understand the origin of CBS, let us consider the situation depicted in figure 1. A sample of randomly distributed scatterers is illuminated by a plane wave (wavelength in vacuum λ, wavevector $\boldsymbol{k}_{\mathrm{in}}$). The quantity of interest is the angular distribution of the scattered light intensity in the backward direction. We consider here the simplest case of scalar waves. Some consequences of the vector nature of the light waves will be discussed in section 3.2.

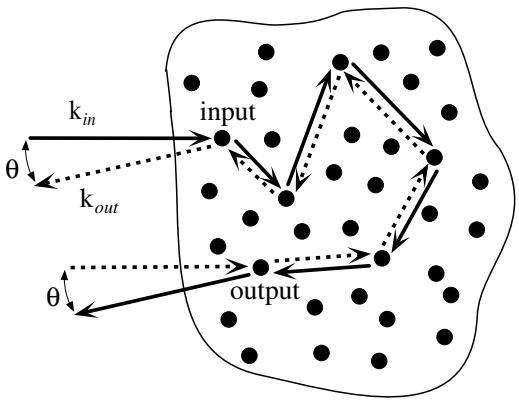

Figure 1. The origin of CBS. The effect arises from the constructive interference in the backscattering direction ($\theta = 0$) between reverse light paths inside the sample. Since the 'direct' (solid arrows) and 'reverse' (dotted arrows) paths are identical for $\theta = 0$, this interference survives configuration averaging.

If the scatterers' respective positions are fixed, the light intensity scattered at angle θ results from the interference of many partially scattered waves and is a fast-varying function of θ. This is the well known speckle pattern (see figure 2(a)). The speckle pattern is observed whether the medium is optically thin, with single scattering being dominant, or optically thick in the multiple-scattering regime. Let us now imagine that a configuration averaging is performed: the respective positions of the scatterers in the sample are modified and the corresponding different speckle patterns are summed up, resulting in an averaged intensity distribution. In experiments, this is obtained either automatically due to the scatterer's motion (e.g. in liquid samples), or by moving the sample so that different configurations are probed. As a result of this averaging process, we expect the speckle pattern to smooth out to give a relatively angle-independent intensity distribution. The main argument in this explanation is that the detected field is the coherent sum of scattered electric fields

$$\boldsymbol{E} = \sum_j \boldsymbol{E}_j \exp(\mathrm{i}\varphi_j). \tag{1}$$

The average detected intensity will then be

$$\langle I \rangle = \left\langle \left| \sum_j \boldsymbol{E}_j \exp(\mathrm{i}\varphi_j) \right|^2 \right\rangle = \sum_j \langle |\boldsymbol{E}_j|^2 \rangle + \sum\nolimits_{j \neq k} \langle \boldsymbol{E}_j \cdot \boldsymbol{E}_k^* \exp(\mathrm{i}\varphi_j - \mathrm{i}\varphi_k) \rangle \tag{2}$$

where the brackets denote configuration averaging. A first approach would be to suppose that the phases φ_j and φ_k are uncorrelated random variables, which yields an interference term equal to zero:

$$\langle I \rangle = \left\langle \sum_j |\boldsymbol{E}_j|^2 \right\rangle. \tag{3}$$

However, this argument is wrong if the interference arises from two *correlated* fields. Such correlations can be very important in the case of spatial correlation of the scatterers, as, e.g. in Bragg scattering in crystals. But even if there is, for example, no correlation in the position of the scatterers, the fields $\boldsymbol{E}_j$ and $\boldsymbol{E}_k^*$ can be correlated. In particular, this is the case for backscattering in the multiple-scattering regime.

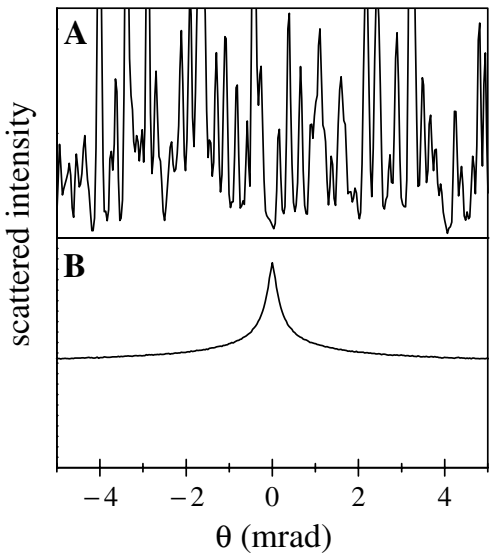

Figure 2. Interference effects and configuration averaging. (a) shows a typical plot for the backscattered angular intensity distribution for one configuration of the sample (speckle pattern). (b) shows the backscattered intensity distribution after configuration averaging (CBS cone).

Indeed, let us consider for every scattering path (yielding some backscattering), the *reverse* path as represented in figure 1. This reverse path (dotted arrows) involves the same scattering sequence as the 'direct' path (solid arrows), but in inverse order. The geometrical phase difference between waves following these two paths is

$$\Delta\varphi = (\boldsymbol{k}_{\mathrm{in}} + \boldsymbol{k}_{\mathrm{out}}) \cdot (\boldsymbol{r}_{\mathrm{in}} - \boldsymbol{r}_{\mathrm{out}}) \tag{4}$$

where $\boldsymbol{r}_{\mathrm{in}}$ and $\boldsymbol{r}_{\mathrm{out}}$ are the vector positions of the first and last scatterers involved in the path (denoted by 'input' and 'output' in figure 1). One can thus see that if the relative position of the scatterers is randomly changing the phase difference is generally also a random parameter and the corresponding interference terms in equation (2) will be cancelled. However, for the particular case of backscattering ($\boldsymbol{k}_{\mathrm{in}} + \boldsymbol{k}_{\mathrm{out}} = 0$) this phase difference is always zero, *regardless of the specific scattering path* considered. Thus, the two waves following the reverse paths of figure 1 always add up constructively in the backscattering direction, and this interference survives the averaging process (this property is of course not verified for $\theta \neq 0$, where the interferences vanish). The remaining terms in equation (2) arise from interference between *distinct* paths and are obviously zero since the fields are not correlated in this case. As a result, the averaged intensity distribution exhibits a peak centred at $\theta = 0$, known as the CBS cone. This is illustrated in figure 2, where the intensity distributions for a given fixed configuration (a) and after configuration averaging (b) are recorded. Note that, in the case of a single configuration (speckle), one does not necessarily have constructive interference in the backscattering direction. The ratio of the configuration-averaged scattered intensity at $\theta = 0$ (exact backscattering) to the 'incoherent background' obtained at a large angle is

known as the CBS enhancement factor. If the amplitudes of the reverse paths, which interfere in the backscattering direction, are equal, the enhancement factor equals 2. However, this property is verified only if the single-scattering light, which does not contribute to CBS, is removed from the detected signal. We will see in section 3.2 how this can be achieved by selecting the appropriate polarization channel.

2.2. Cone shape

The enhanced backscattering described above relies on the constructive interference between reverse paths. One can make an analogy with a Young's interference experiment, where two diffracting slits would be positioned in place of the 'input' and 'output' scatterers (see figure 1). If the slits are backlit with a plane wave (of wavevector $-\boldsymbol{k}_{\mathrm{in}}$), the interference produces a sinusoidal fringe pattern in the far field, with a maximum intensity at $\theta = 0$ and a fringe spacing inversely proportional to the *transverse* spacing between the scatterers (this is valid only for small values of θ). The total configuration-averaged intensity distribution is obtained by summing up incoherently the fringe patterns corresponding to all the possible scattering paths in the sample. This incoherent sum accounts for the fact that interferences between waves following distinct paths do not survive the configuration averaging. Since the fringe patterns all have a 'bright' fringe at $\theta = 0$, the total intensity is maximum there, and decreases to an 'incoherent background' value within an angular range $\Delta\theta \sim \lambda/d$, where d is the average transverse distance between slits (this is similar to the zero-path-difference fringe observed in Michelson interferometers with white light). This analogy thus shows why the average light intensity is increased around the backscattering direction, and relates the angular width of the peak to the inverse of the distance between entry and exit points of the light in the sample.

More precisely, in the case of a semi-infinite medium and for scalar waves, the full-width half-maximum (FWHM) of the CBS cone is given by [8, 9]

$$\Delta\theta_{\mathrm{CBS}} \approx \frac{0.7}{kl^*} \tag{5}$$

where k is the wavevector in the scattering medium, and l^* is the *transport* mean free path. The transport mean free path describes the distance necessary, on average, for the initial direction of propagation to be scrambled (which is of course essential to observe backscattering). It is related to the *scattering* mean free path l (mean distance between two scattering events) by

$$l^* = \frac{l}{1 - \langle\cos\theta\rangle} \tag{6}$$

where θ is the angle between the incident and scattered light (for a single scatterer), and the brackets denote the average over the radiation pattern of the scatterer. Thus, if $\langle\cos\theta\rangle = 0$ the scattering and transport mean free paths are identical. Note that this condition does not imply that the radiation pattern is isotropic (think, for instance, of the dipole radiation pattern).

As was evidenced with the Young's slits analogy, the width of the CBS cone depends on the mean distance between the first and last scatterers. This distance will of course increase with the scattering order N (number of scattering events) involved, so higher orders will yield narrower cones. For large scattering orders ($N \gg 1$) the propagation can be described as a random walk of step l^*, and the average distance between the input and output scatterers grows as $\sqrt{N}l^*$ (diffusion approximation). In a semi-infinite medium where all scattering orders contribute, the total CBS cone is obtained by adding up the cones associated with each order. This implies the evaluation of the weight $P(N)$ of each scattering order. Due to the presence of very high scattering orders (giving very narrow cones), the actual shape of the cone around the tip is triangular [10]. The resulting angular FWHM is given by equation (5). The relationship between cone width and scattering order is illustrated in figure 3(*a*), where the CBS cones associated with $N = 2, 3, 10$ (thin curves) and the sum of all the contributions up to $N = 80$ (bold curve) are plotted, in the case of a slab of non-absorbing medium of optical thickness $b = 12$.

The scattered intensity is plotted as a function of the normalized backscattering angle θkl^*. These curves are obtained with a rigorous theory [11] for scalar waves, which does not rely on the diffusion approximation. Each cone is scaled by its own incoherent background for better comparison of the widths, so the respective amplitudes of the different orders do not appear in this plot. It can be seen that the width of the cone decreases as the scattering order increases (the double-scattering cone is approximately ten times broader than the 'total' peak). The shape is also clearly affected, for instance in the 'wings' of the cones ($\theta kl^* \gg 1$): for $N = 2$, the scattered intensity decreases as $1/\theta$ while the sum of all the other contributions decreases as $1/\theta^2$ [12]. In figure 3(*b*) the weights $P(N)$ corresponding to each scattering order are plotted. Asymptotically, the weight of the Nth-order decreases as $N^{-3/2}$ [11].

Thus, we emphasize that the CBS cone shape is in general determined not only by the transport mean free path, as in the case of a semi-infinite medium (equation (5)), but also by the sample geometry through a truncation of the scattering orders. A similar effect is obtained in the case of an absorbing medium, where the contribution of long light paths is reduced.

3. Experiments with classical scatterers

We now turn to the description of CBS experiments using classical samples such as milk, suspensions of TiO_2 particles, or teflon. We discuss several effects that can affect the CBS signal.

3.1. Description of the experimental setup

The CBS detection setup used in our experiment is schematically represented in figure 4. The sample is illuminated by a collimated laser probe ($1/e^2$ waist 7.6 mm). Most of the backscattered light ($\sim$90%) is reflected by a beam splitter, and its angular (far-field) distribution is recorded on a cooled CCD placed in the focal plane of an analysis

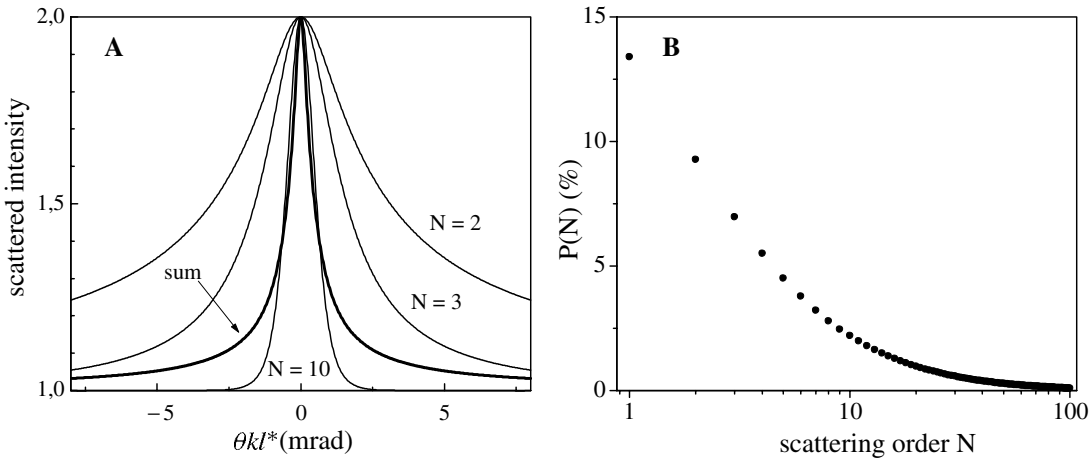

Figure 3. Contribution of different scattering orders N in a slab of optical thickness $b = 12$ (theory). (*a*) CBS cones for $N = 2, 3, 10$ and the sum of the first 80 orders (each cone maximum is scaled to 2, the respective weight of each order is not respected). (*b*) Contribution of each order to the total backscattered intensity.

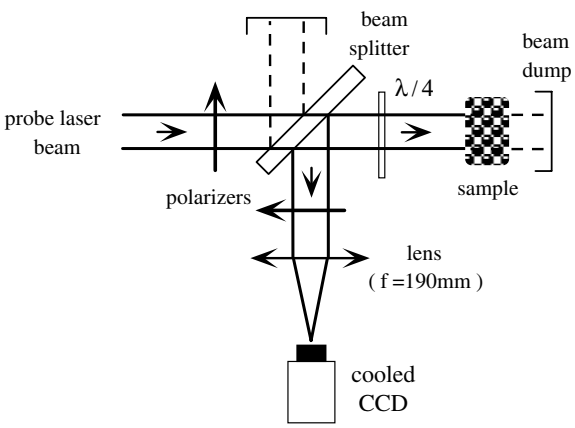

Figure 4. CBS detection setup. The sample is illuminated by a collimated laser beam. The scattered light is collected through a beam splitter and its angular (or far-field) intensity distribution is recorded on a cooled CCD in the focal plane of a lens. Various polarization channels can be selected using polarizers and a quarter-wave plate.

lens ($f = 190$ mm). Since the focusing is quite critical, the CCD camera is mounted on a translation stage. By rotating the polarizer and quarter-wave plate, one can select the polarization channel where the signal is detected (see section 3.1.3).

As usual in CBS experiments, great care must be taken to shield the detector against stray light; the alternative paths that can be followed by the light (incident beam reflected by the beam splitter and beam transmitted by the sample) must also be carefully blocked to avoid any unwanted backscattering. This is achieved by inserting a neutral filter at the Brewster angle in the unwanted beam paths. The residual reflection by the neutral filter is directed onto black paper.

Another possible source of stray light originates from reflections inside the beam splitter. This is avoided by using a beam splitter with a small wedge (5°). This beam splitter has different reflection coefficients for s- and p-polarized light (polarization orthogonal or parallel to the plane of incidence respectively), which have to be accounted for when comparing data in different polarization channels. Another consideration is the angular response of the detection optics (quarter-wave plate + beam splitter + polarizer), which should be sufficiently flat within the angular field of observation to avoid deformation of the background level. However, because of our small detection angular range ($\simeq$15 mrad), this effect is negligible in our case.

The use of a cooled CCD with low thermal (and readout) noise allows for long integration times yielding an improved signal-to-noise ratio. This is also convenient to record CBS cones from self-averaging samples such as milk or a suspension of TiO_2 particles, where the CCD camera integrates the scattered light for several tens of ms up to several minutes, depending on the timescale of the motion of the scatterers.

3.1.1. Angular resolution. To detect CBS cones with a small angular width, it is important to avoid convolution due to the residual divergence of the incident laser beam and to aberrations of the detection optics. The probe beam collimation is achieved using a telescope including a spatial filter, and shear plate interferometry [13] as a diagnostic technique. The diffraction limit corresponding to our beam waist size is $\Delta\theta_{\rm diff} \simeq 0.03$ mrad FWHM, below the resolution limit due to the CCDs pixel size $\Delta\theta_{\rm pix} \simeq 0.05$ mrad. For technical reasons linked to the experiment with cold atoms, the actual detection optics is more complicated than represented in figure 4 and includes an image transport system between the focal plane of the analysis lens and the CCD (see figure 12). All the lenses in the detection system are achromatic doublets to minimize aberrations.

The most direct way to estimate the effective angular resolution of the experimental setup is to record the CBS cone from a liquid sample, milk for instance, which is gradually diluted to increase the scattering mean free path (thus reducing the width of the cone). Once the cone becomes narrower than the angular transfer function of the apparatus, the observed signal is strongly reduced due to convolution and its width is essentially that of the transfer function. Using this procedure, we find an effective angular resolution

$\Delta\theta_{\rm res} \simeq 0.1$ mrad. We believe this value results from residual aberrations in the optical system. Knowing the effective resolution, it is then possible to compute the broadening and reduction of the CBS cone due to convolution.

Although it has many advantages, the choice of a CCD also implies that the angular dynamics of our detection is somewhat limited (the CCD has 770×512 pixels) compared with, for instance, the system of [14]. Because of the far-reaching wings of typical CBS cones, it is difficult to have at the same time an angular magnification (determined by the focal length of the analysis lens) good enough to look at the shape of the cone around the tip, and an angular field wide enough to see the wings.

3.1.2. Signal acquisition and treatment. Here we describe our standard procedure to obtain a CBS cone profile such as that shown in figure 14. First an image of the CBS cone is recorded. The configuration averaging is performed using a small rotor (solid samples) or simply by the motion of the scatterers (liquids, cold atoms). A typical integration time is 20 s. Then, a second 'background' exposure is taken without sample, and subtracted from the signal to remove residual stray light. This step will be discussed in more details in the case of an atomic sample.

Once the image is obtained, a cross section is taken to obtain a profile. However, in the case of a noisy signal, we perform an angular average on the CCD image to smooth the CBS profile: the centre of the CBS peak is pinpointed, and a number of different cross sections passing through this centre are averaged to give the final signal. We emphasize that this technique can only be employed if the cone is isotropic, which is the case only in certain polarization channels (see section 4.3.3). We checked that, in the appropriate channels, this procedure yields the same profile as when using a simple cross section.

The remaining problem is the determination of the enhancement factor, which implies an estimation of the level of the incoherent background. As already mentioned, the wings of the cone are quite wide and a direct measurement of this background level is difficult. Thus, we fit the experimental profile with a sum of four Lorentzian curves, all centred on $\theta = 0$ but with widths and heights as free parameters. The value of the background is also returned by the fit and used to determine the enhancement factor. This empirical approach allows one to fit, using the same procedure, different cone shapes whose analytical expressions are not known. To estimate its accuracy, we applied the technique to two different theoretical cone shapes: a cone from a semi-infinite medium (diffusion theory, $I(\theta) \propto 1/\theta^2$ for $\theta \gg \lambda/l^*$) and a double-scattering cone ($I(\theta) \propto 1/\theta$ for $\theta \gg \lambda/l^*$). For an angular field of detection about 20 times wider than the FWHM of the cones (typical experimental situation), the error in the enhancement factor is below 1%. The actual uncertainty in the enhancement factor originates from the fact that our smoothing procedure does not improve the signal-to-noise ratio at the cone tip, because this particular point is common to all the profiles averaged. To reduce the uncertainty, we average the signal from a few neighbouring pixels around the centre of the cone, but the improvement is limited since the corresponding angular range must remain smaller than the resolution. We finally estimate the uncertainty on the enhancement factor f_e to be around $f_e \pm 0.01$.

3.2. Polarization effects

An important aspect of all CBS experiments with light is the vector nature of the scattered wave, i.e. the polarization of the light. Thus, controlling the incident and detected polarizations is essential in these experiments.

For a linear incident polarization (quarter-wave plate removed), we record (by rotating the detection polarizer) the scattered light either with linear polarization parallel ('parallel' channel or $lin \parallel lin$) or orthogonal ('orthogonal' channel or $lin \perp lin$) to the incident one. We also use a circular incident polarization by inserting the quarter-wave plate between the beam splitter and the sample. In the 'helicity-preserving' channel (denoted $h \parallel h$) the detected polarization is circular with the same helicity (the sign of rotation of the electric field referenced to the direction of wave propagation) as the incident one: in this channel, no light is detected in the case of the back-reflection from a mirror. The 'orthogonal helicity' channel ($h \perp h$) is obtained for a detected circular polarization orthogonal to the previous one. When defining the polarization by referring to a *fixed* axis (as one usually does in the atomic physics community), an incident σ^+ light would remain σ^+ by reflection from a mirror. The $h \perp h$ channel is thus a σ^+/σ^+ channel, and the $h \parallel h$ channel corresponds to a polarization flip from σ^+ to σ^-.

The choice of the appropriate polarization channel makes it possible, at least for some categories of scatterers, to remove the single-scattering contribution to the detected light. Indeed, single scattering does not contribute to CBS but adds up to the signal as a background, and thus reduces the apparent enhancement factor (defined as the ratio of the detected intensities at $\theta = 0$ and $\theta \gg \lambda/l^*$). In the case of single (back)scattering, 'spherical' scatterers, e.g. Rayleigh (size $a < \lambda$) and spherical Mie ($a \gtrsim \lambda$) scatterers, behave like mirrors: they flip the helicity of circularly polarized light. Thus, CBS experiments are usually performed in the $h \parallel h$ channel where the single-scattering contribution is rejected. Furthermore, the reciprocity principle [15] can be used in this channel, and predicts an enhancement factor of 2. In the case, for example, of non-spherical scatterers, the single-scattering contribution is present even in the $h \parallel h$ channel and the expected enhancement factor is smaller than 2 [16].

Polarization can also affect the enhancement factor in more subtle ways. This is illustrated in figure 5 with the example of $N = 3$ scattering and dipole scatterers.

The incident wavevector is orthogonal to the plane of the figure (parallel to $\boldsymbol{e}_z$), where all the scattering events are supposed to take place. We consider the case of detection in the $lin \perp lin$ channel: the incident wave polarization is parallel to $\boldsymbol{e}_x$ and the detected polarization along $\boldsymbol{e}_y$. The arrows mark the polarization of the wave after each scattering. This figure illustrates the fact that the amplitudes of the reverse paths that interfere to give rise to the cone are different in this channel: for the path on the left (scattering sequence $1 \rightarrow 2 \rightarrow 3$) some light comes out in the polarization

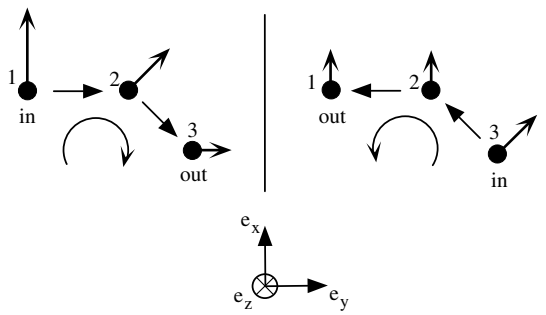

Figure 5. Reduction of the CBS enhancement factor in the $lin \perp lin$ channel. This example illustrates an effect of light polarization on CBS. We consider a scattering path involving three dipole scatterers lying in the plane of the figure. The incident light wavevector is orthogonal to this plane (along $\boldsymbol{e}_z$) and the incident polarization is parallel to $\boldsymbol{e}_x$. We compare the amplitudes of the 'direct' (left, sequence $1 \rightarrow 2 \rightarrow 3$) and 'reverse' (right, sequence $3 \rightarrow 2 \rightarrow 1$) paths after projection on the detected polarization axis $\boldsymbol{e}_y$. The bold arrows denote the light electric field after each scattering event (i.e. the projection of the incident field on the plane orthogonal to the scattering direction). For the 'direct' path on the left, there is a non-zero component of the backscattered electric field along $\boldsymbol{e}_y$. For the 'reverse' path on the right, the backscattered electric field is orthogonal to $\boldsymbol{e}_y$. Thus, the contrast of the interference between the waves following the two paths is reduced.

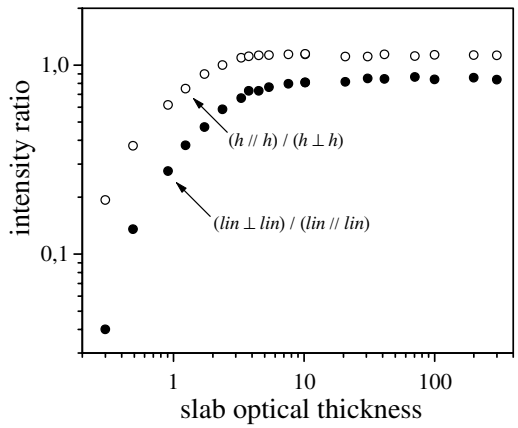

Figure 6. Depolarization due to multiple scattering. This figure shows the measured backscattered intensity ratio (outside of the CBS cone, i.e. the 'incoherent background' value (cf (2.1))) in crossed polarization channels, for a slab of increasing optical thickness. Open circles correspond to circular polarization and solid circles to linear polarization. For small optical thicknesses, the initial polarization is partially retained yielding cross-polarization ratios smaller than unity. For large values of the optical thickness, the light is mostly depolarized yielding a ratio close to unity.

orthogonal to the incident, while for the reverse sequence ($3 \rightarrow 2 \rightarrow 1$) the projection on the detected polarization is zero. Since the amplitudes of the two waves are imbalanced, the contrast of the interference will be reduced and hence so will the CBS enhancement factor. This contrast reduction effect becomes more effective as the order of scattering N increases. Thus, in the case of 'spherical' scatterers, the enhancement factor in the 'orthogonal' channels (linear and circular) is 2 for $N = 2$ [9], and decreases quickly for higher orders. For aspherical scatterers (e.g. antennas), the enhancement factor in the orthogonal channels is smaller than 2 even for $N = 2$.

To summarize, in the case of scatterers of spherical symmetry, the only polarization channel where the enhancement factor is 2 is the helicity-preserving channel ($h \parallel h$) because both the reciprocity principle applies *and* the single-scattering contribution is removed. For non-spherical scatterers, the enhancement is smaller than 2 in all channels.

When multiple scattering occurs, the polarization of the incident wave is rapidly scrambled. This phenomenon is illustrated in figure 6. On this plot we reported the ratio of the intensities scattered in crossed channels for an incident circular polarization (ratio $= I_{h\parallel h}/I_{h\perp h}$, open circles) and linear polarization (ratio $= I_{lin\perp lin}/I_{lin\parallel lin}$, full circles), as a function of the optical thickness of the sample. The sample is a solution of TiO_2 particles (size $\simeq$200 nm) in a cell with a slab geometry (thickness 7 mm). The concentration of the solution is gradually varied to modify the optical thickness of the slab. At low optical thickness, single scattering is dominant and the sample behaves like a 'diffusive mirror': the polarization remains almost unaffected and the scattered light is detected mainly in the $lin \parallel lin$ channel for incident linear light, and in the $h \perp h$ channel for circular light. As optical thickness is increased, higher orders of scattering appear and an increasing amount of light is redistributed in the orthogonal channels. For high values of the optical thickness, the light is almost depolarized and the intensity ratio is close to unity. The fact that the curve for linear polarization is above that for circular light is probably due to the contribution of low scattering orders (which is significant even in a semi-infinite medium [11]). Indeed, it is known that the 'memory' of the initial polarization is preserved longer for linear than for circular polarization in the case of Rayleigh scatterers [17].

3.3. Enhancement factor

The accurate determination of the enhancement factor in CBS experiments is quite delicate [10]. Indeed, the observed enhancement factor is usually quite a bit smaller than the theoretical prediction of 2. This reduction may arise from many causes. We have already mentioned the convolution due to the experimental resolution and the divergence of the probe beam. We also saw, in the previous section, that the theoretical enhancement factor is smaller than 2 in the $lin \perp lin$ and $h \perp h$ channels. Reciprocity predicts an enhancement factor of two in both the $lin \parallel lin$ and $h \parallel h$ channels. This is assuming that single scattering is eliminated, which is possible only in the $h \parallel h$ channel (for spherical or Rayleigh scatterers). Thus, in channels other than $h \parallel h$, the enhancement factor depends *a priori* on the sample geometry and optical thickness.

However, even in the $h \parallel h$ channel, another effect can reduce the enhancement factor. As emphasized by the Young slits analogy, CBS is essentially a two-wave interference effect. What determines the contrast of the interference is the *correlation* between the fields at the input and output scatterer positions. This correlation includes both differences in amplitude and phase of the waves at the two points. For instance, the intensity distribution can be homogeneous and the phase varies in the transverse plane: in

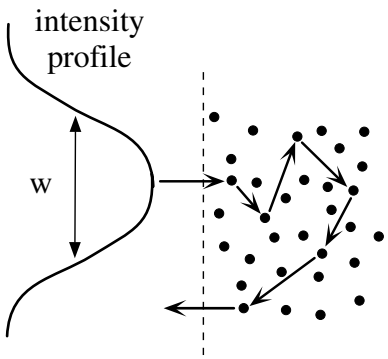

Figure 7. The effect of laser intensity profile on the enhancement factor. In CBS experiments, the sample is illuminated by an inhomogeneous wave such as, for example, a Gaussian beam. If the 'input' and 'output' positions of a given scattering path are separated by a significant amount of the beam diameter, the amplitudes of the 'reverse' light paths are imbalanced and the CBS enhancement factor is reduced.

this situation of partial spatial coherence, the enhancement factor is decreased [18, 19]. In the case of a Gaussian laser beam, the spatial coherence is high and it is rather the inhomogeneous intensity profile that plays a dominant role, as shown in figure 7. If the distance between the first and last scattering event of a given path is larger than the transverse size of the laser beam w, then the amplitudes of the direct and reverse paths are imbalanced and the enhancement factor will be reduced. One expects the reduction effect to be more important for increasing values of l^*/w. In most samples $l^* \ll w$ and this effect remains small. However, we will see in section 4.3.1 that in the case of the atomic sample the above condition is not necessarily fulfilled, and this reduction effect should be considered.

3.4. Role of sample geometry

In the case of a semi-infinite medium, the CBS cone width gives direct access to the transport mean free path l^* through equation (5). However, in the case of a finite medium, this simple relationship does not hold anymore, due to the truncation of long light paths. This yields a higher relative contribution of low scattering orders and hence a broader cone. How strong this broadening is depends on the actual geometry of the sample. For instance, in a spherical sample of diameter D, high scattering orders will be truncated faster than in a slab of thickness $e = D$.

To illustrate the importance of sample geometry, we have reported in figure 8 the results from CBS experiments on spherical samples of polystyrene foam with different diameters.

In figure 8(a) we plot the product $\Delta\theta_{\mathrm{CBS}} kl^*$ (where $\Delta\theta_{\mathrm{CBS}}$ is the cone's angular FWHM) as a function of the 'optical diameter' defined as D/l^*, where D is the diameter of the sample. The value of $l^* \approx 0.18$ mm was deduced from the width of cones from bulk samples using equation (5). The circles correspond to the experiment. The solid curve is the prediction of a rigorous theory [11] for scalar waves and a slab geometry; the horizontal axis thus corresponds, for this curve, to the optical thickness $b = e/l$ where e is the slab thickness (we assume $l = l^*$). The dashed line corresponds to the limit of a semi-infinite medium $\Delta\theta_{\mathrm{CBS}} kl^* \approx 0.7$. One can see that the CBS cone from a spherical sample starts to broaden even at large D/l^* ratio, which reflects the fact that long light paths are truncated faster than in the slab geometry. We will see that in the case of the atomic sample, the symmetry is spherical but with a non-uniform (quasi-Gaussian) density profile; we thus can expect truncation effects to play an important role in this situation. In figure 8(b) the measured enhancement factor is reported, which significantly increases as the sphere's diameter decreases (the peak's height increases by $\sim$15%). Two effects tend to increase the enhancement factor. Due to the truncation of long scattering paths, the cone is broadening and the convolution by the transfer function of the apparatus is decreased. However, this does not seem enough to fully explain the observed increase in enhancement factor. We think that part of this improvement is due to an increasingly uniform illumination of the sample, reducing the imbalance effect shown in figure 7.

3.5. CBS with 'single scattering'

We mentioned in section 3.2 that single scattering does not contribute to the CBS signal. However, there is a situation where average-robust interference effects can be observed with single scattering: the case of an optically thin sample in front of a mirror. This situation is depicted in figure 9 and has been studied in [20].

The scattering medium being optically thin, a certain amount of light reaches the mirror and is reflected. The mirror plays the role of a second scatterer with a very anisotropic radiation pattern due to specular reflection. Figures 9(a) and (b) illustrate two processes that yield constructive interference after configuration averaging. The process depicted in (a) corresponds to the 'usual' backscattering situation, while the example presented in (b) shows that the interference is also constructive at an angle 2α from the incident direction. In the far field, this gives a 'ring' of angular diameter 2α for the enhanced scattered intensity, centred on the direction of the normal to the mirror. The effect can also be understood as double scattering by the 'real' scatterer and its image in the mirror.

This 'single-scattering cone' can be observed when one performs CBS experiments on dilute liquid samples in a glass cell of slab geometry. The 4% reflection from the back of the cell is enough to yield an important contrast in the interference, as illustrated in figures 10(a) and (b).

In this experiment, a dilute solution of TiO_2 particles was placed in a quadrangular glass cell of thickness 7 mm. The optical thickness of the slab was $b = 0.6$. This is not a pure single-scattering situation, but higher scattering orders are not dominant. The images were recorded in the $lin \parallel lin$ channel, with an incident polarization vertical in the plane of the figure. In figure 10(a) the cell was tilted vertically so that the vector normal to the back face points upwards. The image shows the section of the enhanced intensity ring in a narrow angular range around the backscattering direction, which is almost a horizontal line. When the cell is tilted horizontally, we obtain the vertical line figure 10(b). To confirm that the effect arises from scattering, we replaced the

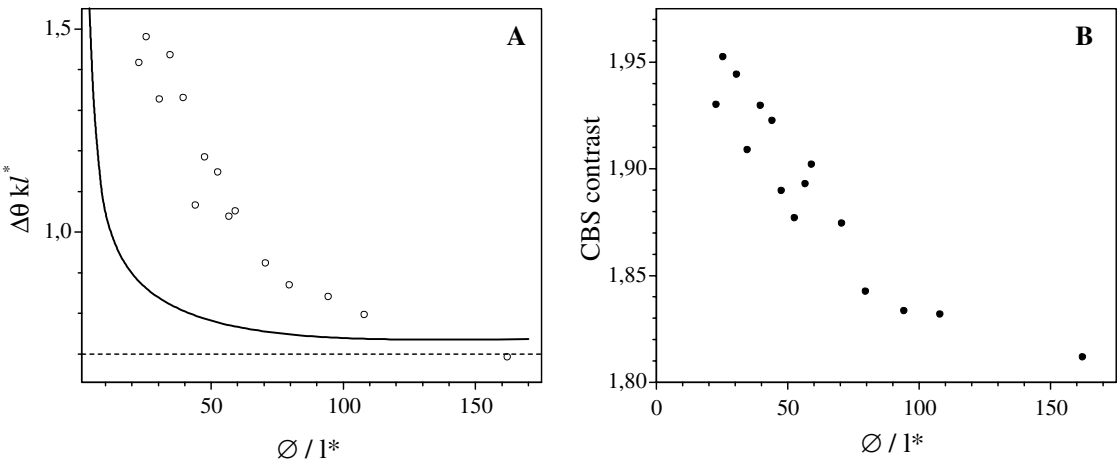

Figure 8. CBS experiments on spherical samples of polystyrene foam (diameter D). (a) shows the measured CBS cone width (in normalized angular units $\Delta\theta kl^*$ where $\Delta\theta$ is the angular width, k the wavevector and l^* the transport mean free path) as a function of D/l^* (open circles), compared with the theoretical cone width for a slab of thickness D (bold curve); the dotted line represents the limit of a semi-infinite medium (see equation (5)). Plot (b) shows the enhancement factor corresponding to the experimental data of (a).

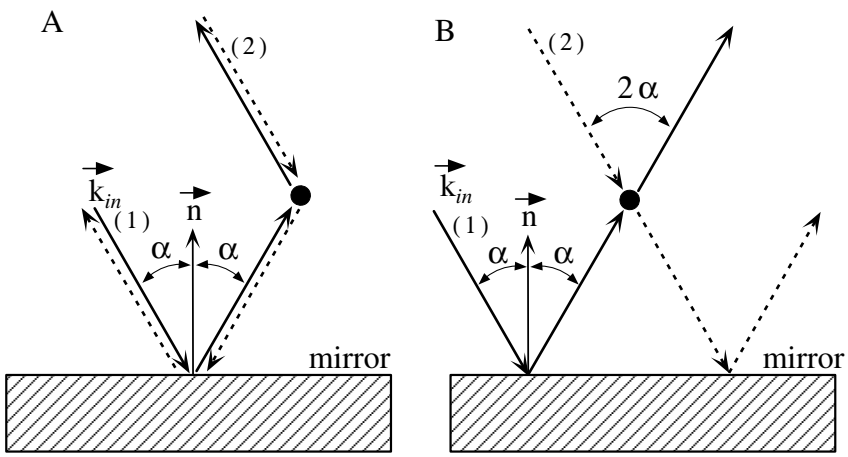

Figure 9. CBS with 'single scattering': the principle. An optically thin sample (single scattering only) is placed in front of a mirror tilted with respect to the direction of incidence by an angle α. Figures (a) and (b) illustrate two processes yielding constructive interference resisting configuration averaging (i.e. over the scatterer-mirror distance). (a) 'Standard' backscattering configuration, where the mirror plays the role of the second scatterer. (b) 'Forward' scattering yielding a constructive interference at an angle 2α from incidence. These interferences yield a ring-shaped angular distribution of diameter 2α, centred on the direction normal to the mirror plane.

solution in the cell by pure water, and the ring disappeared. Since the process involves only single scattering (and the reflection from a mirror), the polarization is preserved around the backscattering direction. Thus, when we recorded the backscattered intensity in the $lin \perp lin$ channel, the ring also disappeared.

It is thus possible with this configuration to study an interference effect very similar to CBS, but in the single-scattering regime. This is an interesting possibility in the case of an atomic sample, as the theory becomes much simpler.

4. Experiments with cold atoms

4.1. Properties of atomic scatterers

CBS constitutes a new tool to probe the properties of cold atoms. Indeed, atoms as elementary scatterers are an interesting medium to study the quantum manifestations of the interaction between light and matter. As a consequence of the discrete energy levels, the atom's scattering cross section is highly resonant ($Q \approx 10^8$) and the resonance frequency is identical for all the scatterers in the sample (assuming a negligible Doppler effect, which implies laser cooling). Such a situation would be very difficult to achieve with classical resonators such as, for instance, dielectric spheres of high finesse. Due to this narrow resonance, the light mean free path in the atomic medium can be varied by orders of magnitude by shifting the wave frequency a few linewidths away from the atomic transition. As we will see in section 4.3.1, the presence of an internal structure in the ground state (Zeeman sublevels) has some other profound consequences on the CBS signal from the atomic sample used in our experiment.

Several reasons motivate the use of *cold* atoms to observe CBS. Firstly, Doppler broadening is then reduced and all the atoms have the same resonant scattering cross section,

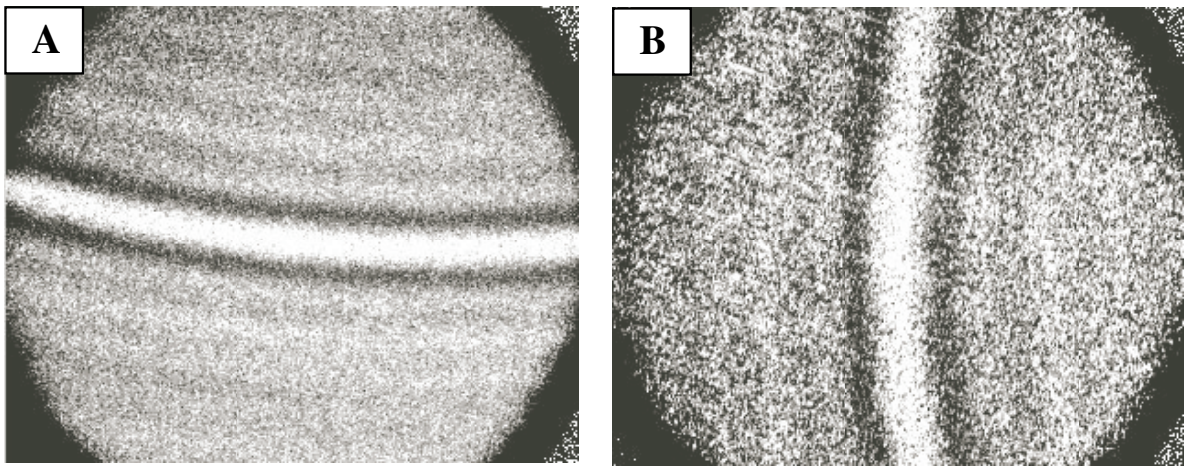

Figure 10. CBS with 'single scattering': the experiment. These images show the far-field distribution of the backscattered light from an optically thin slab in front of a mirror. (*a*) Mirror tilted vertically. (*b*) Mirror tilted horizontally.

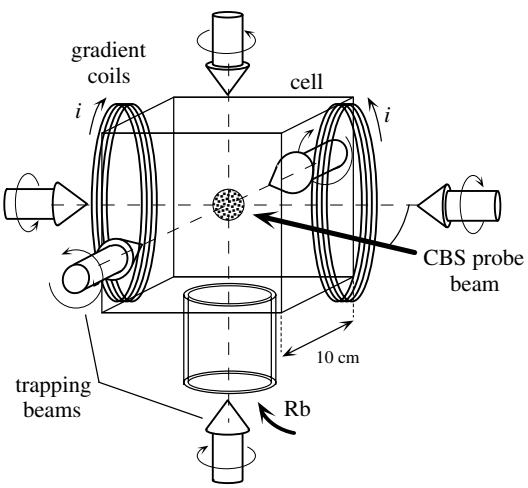

Figure 11. Setup of the MOT. Rubidium 85 atoms from a dilute vapour in a quartz cell are trapped and cooled by the magneto-optical force exerted by six independent laser beams in a magnetic field gradient. The CBS laser beam sent through the cold atomic cloud lies in the horizontal plane, at an angle of 25° from one of the trapping directions.

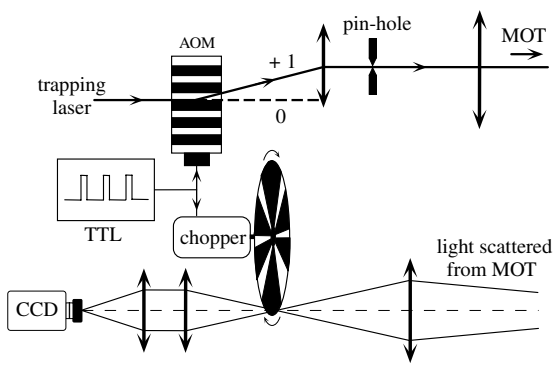

Figure 12. Synchronization of the detection. To observe CBS, one needs to release the atoms from the trap. Thus, in our experiment, the MOT is turned on for 20 ms and then switched off for 3 ms (using an acousto-optic modulator) while the CBS signal is recorded. To achieve this high duty cycle, we continuously leave the CCD in the 'exposure' mode, and a synchronized chopper is used to shield the CCD from the bright fluorescence light emitted during the MOT phase.

characterized by the natural width Γ of the atomic transition ($\Gamma/2\pi \approx 6$ MHz for rubidium). However, the atom's motion has a more important consequence on CBS: if the motion of the scatterers is fast compared with the time for the scattered wave to pass through the medium, the two reverse waves of figure 1 will encounter different configurations, resulting in a 'dynamic' break down of reciprocity. For non-resonant scatterers, the typical timescale to consider is the propagation time between two scattering events, so this effect requires extremely fast (almost relativistic) motion [21]. In the case of resonant scattering by atoms, however, the timescale is considerably increased by the on-resonant scattering delay time $\tau_{\rm res} = 2/\Gamma$ [22]. Taking as a criterion for the break down of the CBS cone that each scatterer has moved by one wavelength during that typical timescale

$$\Delta x = v\tau_{\rm res} \gtrsim \lambda \tag{7}$$

one requires to observe CBS velocities smaller than

$$v_{\rm crit} \backsim \frac{\lambda}{\tau_{\rm res}} = \frac{\lambda\Gamma}{2}. \tag{8}$$

In terms of Doppler broadening, this corresponds to

$$kv_{\rm crit} \backsim \Gamma. \tag{9}$$

The above criterion shows that if one employs resonant laser light on a dilute atomic gas (to maximize the optical thickness of the sample and favour multiple scattering), one has first to laser-cool these atoms in order to observe CBS. For rubidium atoms, satisfying condition (9) implies cooling down the atomic sample below $T_{\rm crit} = 0.25$ K, a regime easily reached by standard techniques.

An alternative picture to the time argument developed above is to consider that an incoming monochromatic plane wave experiences a phase shift due to scattering by an atom. This shift depends on the light frequency in the atom's inertial

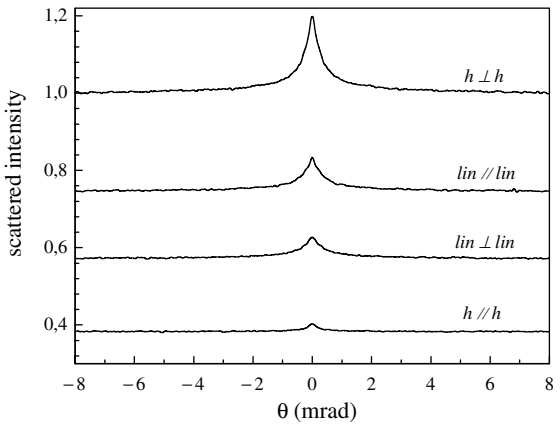

Figure 13. Atomic CBS profiles (after angular average) in the four polarization channels. All profiles have been scaled by the same value, so that the incoherent background in the $h \perp h$ channel is equal to unity. The enhancement factors are 1.2 ($h \perp h$), 1.06 ($h \parallel h$), 1.12 ($lin \parallel lin$) and 1.10 ($lin \perp lin$). The width of the cone in the $h \perp h$ channel is 0.6 mrad.

frame, thus it is sensitive to the atom's motion via the Doppler effect. Thus, a light wave following a certain multiple-scattering path can be seen as receiving a succession of random phase 'kicks'; the total phase accumulated will be different for the direct and reverse paths of figure 1, yielding a reduced contrast of the interference [23]. By imposing the condition that the phase difference is smaller than π, one naturally recovers criterion (9), for a single-scattering event. In the case of a scattering order $N \gg 1$, one expects the phase difference between reverse paths to grow as $\sqrt{N}$, imposing a critical temperature decreasing as $1/N$.

In light of the phase-shift picture just discussed, one can reasonably expect the effect of the atom's motion on CBS to decrease when the laser is detuned from resonance. Indeed, for large detunings, the resonant character of the atomic scatterer vanishes and one recovers the situation discussed in [21]. However, some theoretical work remains to be performed to quantitatively understand the effect of laser detuning on CBS.

4.2. Preparation of the atomic sample

The first step in our experiment is to prepare an atomic sample dense enough to reach the multiple-scattering regime. The relevant parameter is the optical thickness of the atomic cloud b. To study multiple scattering of light in the atomic medium, one typically needs $b > 1$.

A MOT is loaded from a room-temperature vapour of rubidium atoms in a quartz cell, as shown in figure 11.

The atoms are trapped by six independent laser beams: this configuration (instead of the usual three retro-reflected beams) allows one to avoid the imbalance in the trapping beams' intensity due to the high optical thickness, and thus to obtain stable trapping. The beams' parameters are: wavelength $\lambda = 780$ nm (D2 line of rubidium), detuning from resonance $\delta \approx -3\Gamma$, diameter 2.8 cm (FWHM) and power per beam 30 mW. The large beam size increases the number of trapped atoms, but requires more laser power. These trapping beams are obtained by splitting a single 200 mW beam, produced by single-pass amplification of a 4 mW beam through a tapered amplifier (SDL TC30-E). The source laser diode is injection-locked to a reference DBR laser diode (Yokogawa YL78XNW/S, $\sim$1 MHz spectral linewidth). A magnetic field gradient of typically 10 G cm^{-1} is applied to spatially confine the cold atoms. The CBS laser probe lies in the horizontal plane of the figure, at an angle of approximately 25° from the trapping beam.

To characterize the atomic cloud, we record the fluorescence from the detuned CBS laser probe on a photodiode and a CCD; we also measure the transmission T of a smaller laser probe (diameter $\simeq$1 mm) sent through the centre of the atomic cloud to determine its optical thickness $b = -\ln(T)$. When using this method, one should make sure that most of the probe laser power lies in a spectral range much narrower than the natural width Γ; the residual power outside this range will appear as an offset in the transmitted power, yielding an underestimated value for the optical thickness. By filtering our laser probe with a Fabry–Perot cavity, we are able to measure optical thicknesses up to approximately 9 (in a cell of heated rubidium gas). However, the reader should keep in mind that these values are still underestimated. For a Gaussian atomic density profile of peak value n_0 and waist w (half-width at $1/e^2$), the optical thickness is $b_0 = \sigma n_0 w\sqrt{\pi/2}$. The MOT loading time is typically around 0.6 s. It contains 1–2 $\times$ 10^9 atoms with a quasi-Gaussian spatial distribution of width typically 6 mm FWHM. Transmission measurements using the $3 \rightarrow 4$ transition of the D2 line yield a typical optical thickness $b \simeq 6$. The temperature of the cloud is measured by time of flight. The rms velocity of the atoms is 10 cm s^{-1}, small enough to fulfil the criterion (9).

To observe the CBS cone, we have to turn off the MOT trapping beams. This is because the fluorescence of the atoms excited by the trapping lasers (total scattered power $\simeq$4 mW!) is much brighter than the light scattered from the probe. Also, it seems preferable to avoid perturbations of the atoms by the trapping lasers during the CBS measurement. Thus, we alternate a 'MOT phase' (duration 20 ms) where the atoms are trapped, with a 'CBS' phase (2–3 ms) where the trapping beams, repumper and magnetic field are switched off (switch-off time <0.2 ms), and the CBS signal is recorded; this phase is sufficiently short so that all the atoms remain in the capture zone and are efficiently recaptured when the MOT is switched back on. In fact, what limits the duration of the CBS phase is the maximum number of photons that can be scattered by each atom before it is 'pushed' out of resonance due to momentum transfer or pumped to the $F = 2$ hyperfine level. For our rubidium atoms, this requires around 1000 photons, which are scattered within 5 ms for a saturation parameter $s_0 = 0.01$ (on-resonance saturation parameter $s_0 = I/I_{\rm sat}$, where I is the laser intensity and $I_{\rm sat} = 1.6$ mW cm^{-2} the saturation intensity for rubidium). With the 'duty cycle' described above, the number of atoms in the trap is stationary and we can chain many such cycles. One problem is that the CCD camera which detects CBS cannot be triggered at such a high rate. The CCD remains all the time in the 'acquisition' mode and thus has to be protected from the bright light scattered during the MOT phase. This is achieved using a chopper wheel as shown in figure 12.

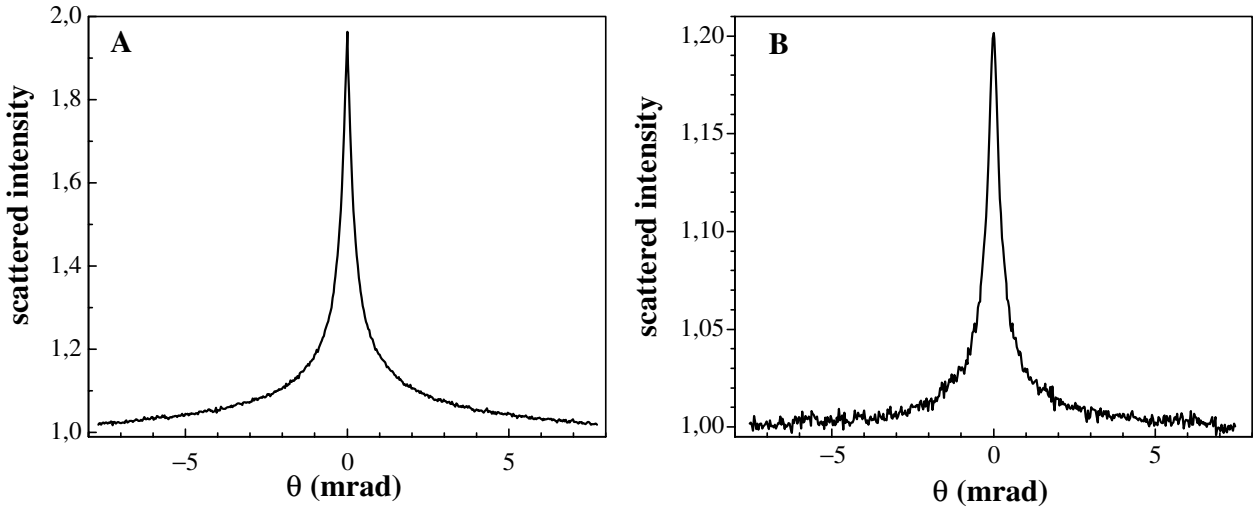

Figure 14. CBS cones from (*a*) a sphere of polystyrene foam ($h \parallel h$), (*b*) the atomic cloud ($h \perp h$). This comparison shows that the reduced enhancement factor observed for the atomic signal is not due to poor angular resolution.

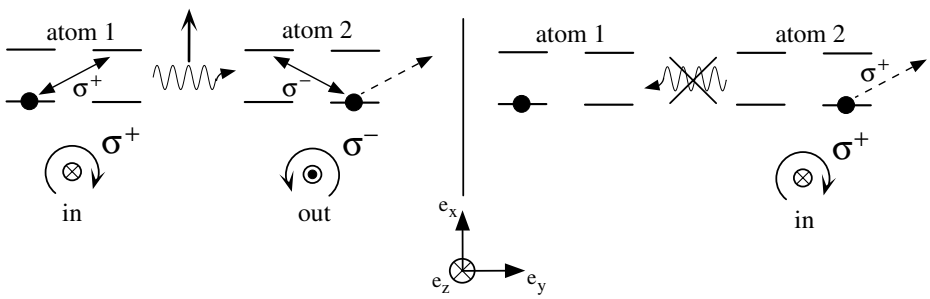

Figure 15. Reduction of the enhancement factor due to the atom's internal structure. This example illustrates a reduction effect due to the internal structure of the atomic scatterer. As in figure 5 the scatterers are in the plane of the figure, and the incident light wavevector is orthogonal to this plane. Here, we consider double scattering only and a $\frac{1}{2} \rightarrow \frac{1}{2}$ transition (but the principle remains essentially the same for a $3 \rightarrow 4$ transition). The two atoms are in different Zeeman sublevels. We also use in this example the $h \parallel h$ channel, so the incident polarization is, e.g., σ^+ and the detected polarization σ^- (same helicity). We compare the amplitudes of the 'direct' (left, sequence $1 \rightarrow 2$) and 'reverse' (right, sequence $2 \rightarrow 1$) paths. Let us consider the 'direct' path. Atom 1 can make a σ^+ transition and radiate a linear polarization towards atom 2; this is seen as a superposition of σ^+ and σ^- light, and atom 2 can scatter σ^- light which is detected. Thus, the amplitude for this path is non-zero. This is obviously not the case for the reverse path (right), since atom 2 cannot scatter the incoming σ^+ light. Thus, the atom's internal structure yields in this case an imbalance of the interfering path amplitudes, and thus a reduction of the CBS enhancement factor.

The chopper is placed in the focal plane of the analysis lens. A transport system images this focal plane on the CCD. The trapping laser is turned on and off with an acousto-optic modulator (residual power 0.2 μW per beam). The same TTL signal is used to drive the modulator and as a reference for the controller of the chopper. The phase is adjusted so that the chopper blades block the detection path when the trapping laser is on. With this system, we are able to take exposures up to several tens of minutes. A typical total exposure time is 1 min, with a detected flux of photons between 140 and 1400 photons/pixel s^{-1}.

It is necessary to acquire a 'background' image without cold atoms to subtract stray light. However, this procedure is more critical than in the case of classical samples, because this stray light originates from different sources. For instance, one could take the background exposure with no magnetic field gradient applied during the MOT phase, which prevents the trapping. However, in this case, a molasse is still operating during the MOT phase that produces a sample of cold atoms (with density increase in velocity space). To avoid this, one needs to turn off either the repumper or the trapping beams to take the background exposure. In this situation, the background signal originates essentially from scattering of the probe beam due to hot atoms in the cell.

4.3. Results

4.3.1. Discussion of the atomic CBS signal. Figure 13 shows the profiles of the atomic CBS cones in the four polarization channels (after angular average). The detected intensity has been scaled so that the incoherent background of the $h \perp h$ curve is equal to unity. In this experiment, the on-resonance optical thickness measured through the centre of the trap is $b \simeq 6$ for a quasi-Gaussian cloud profile of diameter $D \simeq 4$ mm FWHM in the probe direction, yielding a peak density of about 10^{10} cm^{-3} and a scattering mean free path $l \simeq 0.7$ mm at the centre of the trap. A low-intensity probe beam was used, yielding an on-resonance saturation parameter $s_0 = 0.01$. The total exposure (including the 'dark' periods) lasted 160 s.

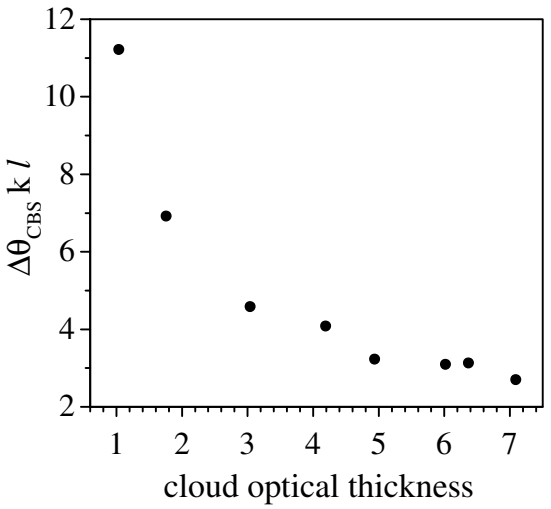

Figure 16. Effect of cloud optical thickness on the width of the CBS cone. We report on this plot the normalized CBS cone width $\Delta\theta_{\mathrm{CBS}}kl$ as a function of the optical thickness at the centre of the atomic cloud. The CBS data are recorded in the $h \perp h$ polarization channel. The size and density of the atomic cloud are varied by adjusting the repumper light intensity. For each data point, the density profile (fluorescence imaging) and optical thickness (transmission) are measured, allowing for the computation of the scattering mean free path l. It varies from 0.4–2 mm in this experiment. The normalized cone width decreases with increasing optical thickness, as observed with 'classical' samples of slab and spherical geometry (see figure 8). The measured enhancement factor is approximately independent of the optical thickness.

The values of the enhancement factor are 1.20 ($h \perp h$), 1.06 ($h \parallel h$), 1.12 ($lin \parallel lin$) and 1.10 ($lin \perp lin$) respectively. The cone width is about 0.6 mrad FWHM in the $h \perp h$ channel. We thus observe that *the enhancement factor is much smaller than 2 in all polarization channels*. Even more striking, the enhancement is only 1.06 in the $h \parallel h$ channel, where reciprocity predicts a value of two for classical (and spherical) scatterers. It is clear that this reduction cannot be attributed to the angular resolution of the apparatus. For a cone width of 0.6 mrad, we expect a reduction of the enhancement by 5% at most. This is confirmed by the observation of a CBS cone from a sphere of polystyrene, which has about the same width as the atomic cone (figure 14). The enhancement factor here is 1.96.

The explanation of this phenomenon lies in the atom's internal structure of the ground state. First, because our atom is not a two-level system (or a $0 \rightarrow 1$ transition), it has a non-negligible probability to make 'spontaneous Raman' transitions between degenerate Zeeman sublevels. In such a scattering event, the atom's internal state (here the Zeeman sublevel of the ground state) after the scattering is different from the initial state, and the polarization of the scattered light differs from the incident one. Thus, for most transitions, the single-scattering contribution cannot be rejected even in the $h \parallel h$ channel. In this respect, atoms behave similarly to strongly non-spherical classical scatterers (like, e.g., oblate dielectric spheroids).

A more subtle effect is an imbalance between the amplitudes of the reverse paths that interfere to give the CBS cone. This is illustrated by the simple example in figure 15: we consider double scattering by atoms with a $\frac{1}{2} \rightarrow \frac{1}{2}$ transition, in the $h \parallel h$ channel. The quantification axis is taken along the wavevector of the incident laser light (parallel to e_z). The incident light is polarized, e.g. σ^+ and only the σ^- component of the scattered light is detected in the $h \parallel h$ channel. We suppose that the two atoms are in different Zeeman sublevels. We only consider the case of Rayleigh scattering (no change of Zeeman sublevel). In the first path (sequence $1 \rightarrow 2$, left), atom 1 makes a σ^+ transition and radiates some light toward atom 2 with a linear polarization parallel to e_x. This is seen by atom 2 as a superposition of σ^+ and σ^- light; since a σ^+ transition is not available, only σ^- light is backscattered and detected in the $h \parallel h$ channel. In the reverse path (right), there is no possibility for atom 2 to make a σ^+ transition: the amplitude of this path is zero. This is of course an extreme situation, but calculations [24] indicate that this effect strongly reduces the enhancement in the various channels. These calculations assume double scattering in a semi-infinite medium, low saturation, a uniform distribution in the ground state Zeeman sublevels, and do not include optical pumping effects. Both Rayleigh and Raman transitions are included, the latter also contributing to CBS. A detailed presentation of these calculations will be reported elsewhere [24]. The results for a $3 \rightarrow 4$ transition are summarized in table 1.

Table 1. Various componants of the atomic CBS signal (theory). This table compares the 'crossed', 'ladder' and single-scattering terms as well as the resulting enhancement factor in the four polarization channels for an atomic sample. The model is for a $3 \rightarrow 4$ transition in the weak saturation limit, and assumes an uniform repartition in the ground state sublevels. The scattering medium is supposed semi-infinite, and only the double-scattering contribution is taken into account. The experimental values of the enhancement factor are reported in the last line for comparison.

	$h\|\|h$	$h\perp h$	$lin\|\|lin$	$lin\perp lin$
γ_c	0.028	0.154	0.108	0.075
γ_l	0.131	0.216	0.180	0.167
γ_s	0.040	0.510	0.348	0.201
Enhancement (theory)	1.166	1.213	1.204	1.206
Enhancement (exp)	1.06	1.20	1.12	1.10

Table 1 contains the contributions to the bistatic coefficient [25] of the 'crossed' (or interference) term γ_c, 'ladder' (or incoherent) term γ_l, and single-scattering term γ_s at exact backscattering ($\theta = 0$). The effective enhancement factor in the presence of single scattering is then

$$\text{enhancement} = \frac{\gamma_c + \gamma_l + \gamma_s}{\gamma_l + \gamma_s} = 1 + \frac{\gamma_c}{\gamma_l + \gamma_s}. \qquad (10)$$

We also reported in the last row the experimental values for comparison. Even though the model considers only double scattering and a semi-infinite medium, the values given in table 1 are surprisingly close to the experimental observations. They reproduce the order of magnitude of the enhancement factor and even the hierarchy between the different channels (for instance, the enhancement is predicted to be smallest in the $h \parallel h$ channel). Note that the reduction of the CBS enhancement factor has different origins in different channels: in the $h \parallel h$ channel, most of the reduction stems from the imbalance mechanism shown in

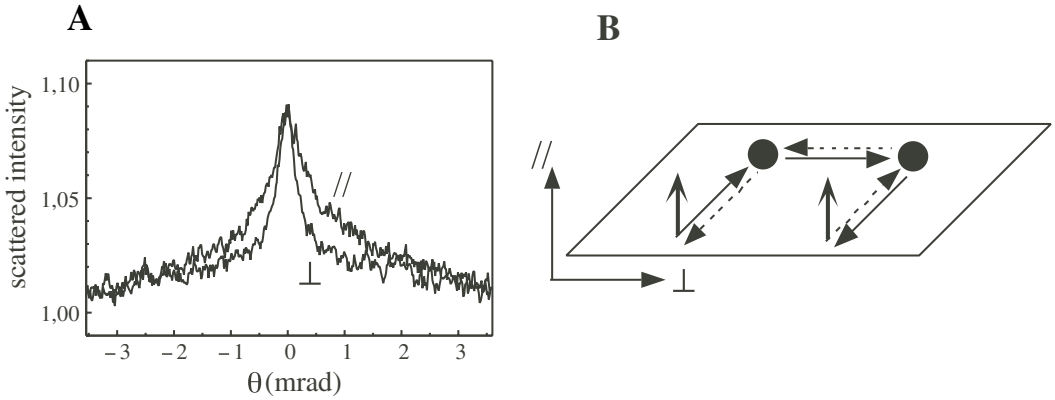

Figure 17. Anisotropy of the CBS cone in the $lin \parallel lin$ channel. (*a*) Experimental observation. This figure shows two cross sections of the CBS cone, respectively parallel and orthogonal to the incident polarization. The parallel cross section is clearly wider. (*b*) Origin of the anisotropy. We assume double scattering only and a linear (vertical) incident polarization. For dipole scatterers, most light will be scattered in the horizontal plane and most double-scattering paths will lie in this plane. Thus, the state of interference will vary slowly when an angular scan is performed along the vertical (broad cone), and faster when the scan is horizontal (narrow cone for a scan orthogonal to the incident polarization).

figure 15 ($1+\gamma_c/\gamma_l = 1.214$), while a strong single-scattering contribution explains most of the enhancement reduction in the $h \perp h$ channel.

The angular width of the atomic cone is $\Delta\theta_{\mathrm{CBS}} \approx 0.6$ mrad. This value is about five times larger than what is obtained with equation (5) and the estimated mean free path of 0.7 mm at the centre of the trap (overestimated, see remark on optical thickness in section 4.2). This is not surprising, since our sample is still far from a semi-infinite medium. However, the relatively high value of 6 for the optical thickness indicates that scattering orders higher than two are present and should be included in a quantitative analysis of the signal. This issue will be discussed further in the next section.

4.3.2. Effect of cloud density. By varying the trap parameters, e.g. the intensity of the repumper laser during the MOT phase, we can modify to a certain extent the characteristics of the atomic cloud (size and density). This modifies the width of the CBS cone, as shown in figure 16.

In this experiment, the value of the repumper intensity was varied; this acts on the number of trapped atoms and on the size of the cloud. The optical thickness and fluorescence profile of the atomic cloud were recorded for each value of the repumper intensity. The measured CBS enhancement factor remained roughly constant. We report in figure 16 the normalized CBS cone width $\Delta\theta_{\mathrm{CBS}}kl$, where the scattering mean free path l at the centre of the cloud was computed using the optical thickness and density profile measurements; these widths are plotted as a function of the optical thickness, as was done in figure 8. We can see that the normalized CBS width decreases as the optical thickness increases, a behaviour qualitatively similar to that of slabs and spheres of uniform density (figure 8). However, the situation here is more complex, since there is a distribution of mean free paths due to the non-uniform atomic density in the cloud. Thus, a numerical computation of the contribution of various scattering orders is required to quantitatively understand these data. A Monte Carlo simulation, including polarization and internal structure effects, is currently being implemented to address this question.

4.3.3. Dipole versus isotropic radiation pattern. We have mentioned above that the CBS cone is not always isotropic. Indeed, we observed some anisotropy on the atomic signal recorded in the $lin \parallel lin$ channel. This is illustrated in figure 17(*a*) where we reported two cross sections of the cone: ($\parallel$) cross section parallel to the direction of the incident polarization, and ($\perp$) cross section orthogonal to the polarization. The first profile is clearly wider (by approximately a factor of two).

This effect, which has already been reported with classical Rayleigh scatterers [9], is due to the combination of low scattering orders and a dipole-type radiation pattern for the atomic scatterer. Indeed, if we consider for instance only double scattering and an incident vertical linear polarization, most of the scattering paths will lie in the horizontal plane because very little light will be radiated in the vertical direction (figure 17(*b*)). Thus, the phase difference between reverse paths will vary much more slowly in the vertical angular direction (where the detector moves along a fringe of the equivalent Young's interference pattern) than in the horizontal one (motion orthogonal to the fringe system), yielding an asymmetric cone.

5. Conclusion

In this paper, we discussed in detail our experiment of CBS of light from cold atoms. Particular attention was drawn to the influence of the sample and laser probe geometry on the CBS signal, as illustrated by experiments on classical samples. The small enhancement factors observed in the experiment on cold atoms are explained by two effects due to the atom's internal structure: the presence of single scattering (spontaneous Raman transitions), and a more interesting imbalance effect in the amplitudes of the time-reversed paths. We are currently setting up a Monte Carlo simulation to take into account the specific geometry of our sample

together with the internal structure properties of the atomic scatterer. Once this necessary tool is developed, we plan to quantitatively study the effect of various parameters such as different atomic transitions, laser frequency and intensity, or an applied magnetic field.

Acknowledgments

We thank the CNRS and the PACA Region for financial support. We also thank the Groupe de Recherche PRIMA of CNRS. We gratefully acknowledge the important contributions of D Delande and T Jonckheere to the theoretical work and numerical simulations, and of J-C Bernard to the development of the experiment.

References

[1] Anderson P W 1958 *Phys. Rev.* **109** 1492–505
[2] Genack A Z and Garcia N 1991 *Phys. Rev. Lett.* **66** 2064–7
[3] Wiersma D S, Bartolini P, Lagendijk A and Righini R 1997 *Nature* **390** 671–3
[4] Kuga Y and Ishimaru A 1984 *J. Opt. Soc. Am.* A **8** 831
Wolf P E and Maret G 1985 *Phys. Rev. Lett.* **55** 2696
van Albada M P and Lagendijk A 1985 *Phys. Rev. Lett.* **55** 2692
Yoo K M, Tang G C and Alfano R R 1990 *Appl. Opt.* **29** 3237–9
Mishchenko M I 1993 *Astrophys. J.* **411** 351–61
Tourin A, Derode A, Roux P, van Tigelen B A and Fink M 1997 *Phys. Rev. Lett.* **79** 3637–9
[5] Labeyrie G, de Tomasi F, Bernard J-C, Müller C A, Miniatura C and Kaiser R 1999 *Phys. Rev. Lett.* **83** 5266
[6] Sesko D W, Walker T G and Weiman C E 1992 *J. Opt. Soc. Am.* B **8** 946
[7] Fioretti A, Molisch A F, Muller J H, Verkerk P and Allegrini M 1998 *Opt. Commun.* **149** 415–22
[8] Akkermans E and Maynard R 1985 *J. Physique Lett.* **46** L-1045
[9] van Albada M P, van der Mark M B and Lagendijk A 1987 *Phys. Rev. Lett.* **58** 361
[10] Wiersma D, van Albada M, van Tiggelen B and Lagendijk A 1995 *Phys. Rev. Lett.* **74** 4193
[11] van der Mark M B, van Albada M P and Lagendijk A 1988 *Phys. Rev.* B **37** 3575
[12] van Tiggelen B A, Lagendijk A and Tip A 1990 *J. Phys.: Condens. Matter* **2** 7653–77
[13] Murty M 1964 *Appl. Opt.* **3** 531
[14] Wiersma D S, van Albada M P and Lagendijk A 1995 *Rev. Sci. Instrum.* **66** 5473
[15] van Tiggelen B A and Maynard R 1997 *Wave Propagation in Complex Media* ed G Papanicolaou *International Mathematical Association* (New York: Springer)
[16] Mishchenko M I 1992 *J. Opt. Soc. Am.* A **9**
[17] MacKintosh F C, Zhu J X, Pine D J and Weitz D A 1989 *Phys. Rev.* B **40** 9342
[18] Lenke R and Maret G *Scattering in Polymeric and Colloidal Systems* ed W Brown and K Mortensen (London: Gordon and Breach) at press
[19] Okamoto T and Asakura T 1996 *Opt. Lett.* **21** 369
[20] Greffet J-J 1991 *Waves Random Media* **3** S65
[21] Golubentsev A A 1984 *Sov. Phys.–JETP* **59** 26
[22] Lagendijk A and van Tiggelen B A 1996 *Phys. Rep.* **270** 167
[23] Jonckheere T and Delande D Private communication
[24] Jonckheere T, Müller C A, Kaiser R, Miniatura C and Delande D 2000 *Phys. Rev. Lett.* submitted
[25] Ishimaru A 1978 *Wave Propagation and Scattering in Random Media* vol 1 and 2 (New York: Academic)